13th ewtec 2019 Proceedings of the 13th European Wave and Tidal Energy Conference 1-6 Sept 2019, Naples, Italy

Definition of metrics and significance hydrodynamic mode-maps for BEM mesh convergence analysis

Simone Giorgi, Ronan Costello and Ben Kennedy

Abstract—**In the topic of wave energy converter (WEC) modelling, boundary element methods (BEMs) are one of the most utilised tools, especially in the early-stage device design. The accuracy of BEM calculation increases by reducing the mesh panel size, however, there is a consequential increase of the computation time. The balance between the required accuracy and the computation time has to be the result of a pragmatic compromise. The utilised mesh can be considered sufficiently fine, if a further mesh resolution increment does not bring significant changes in the calculated BEM hydrodynamic curves. In the case of multiple body WECs or WEC arrays, the number of the hydrodynamic curves to visually inspect could be excessively large, making the inspection too arduous and time consuming. This paper proposes the definition and the use of a metric, to be applied to the BEM results, in order to implement an automatic convergence analysis, to assist with mesh resolution optimization. In the case of a large number of bodies, wave radiation and scattering can generate unexpected interaction effects between the different modes of the system; therefore, the paper also proposes the definition and use of "significance hydrodynamic mode-maps", in order to visualize the most relevant modes of the multiple body system. The paper presents the use of the defined tools in the study of a floating body array, illustrating the calculation of the most significant modes of the system and the optimum compromise for the BEM mesh resolution.**

Index Terms—**BEM, boundary element methods, mesh convergence, potential theory, wave energy**

I. Introduction

IT is well known that most of the physical and engineering problems can be described as a boundary value problem (BVP), which consists of a region of interest characterised by a differential equation, and a set of boundary conditions. The unique solution of the BVP has to satisfy both the differential equation and the boundary conditions [1] [2]. In most cases, BVPs can not be solved analytically, so that a numerical solution methodology has to be employed. Common techniques, utilised to resolve the BVP, are boundary element methods (BEMs), also referred to as panel methods, and finite element methods (FEMs). In the case of FEMs, the whole 3D spatial domain is divided into small volumes (the elements) by utilising a geometrical mesh, in contrast to BEMs, in which the spatial discretization is performed only at the bounding surface, by generating small surface elements. Therefore, BEMs, compared to FEMs, lead to a more efficient computation and less required computer memory, thanks to a reduction of the equation system dimension [3]. In numerical modelling, the mesh preparation is one of the most demanding processes [4]; since BEMs require the mesh of the only bounding surface, the mesh preparation is more cost effective [3] [5]. Furthermore, the adjustment of the mesh is more efficient with BEMs, in the case of problems involving moving boundaries [3].

In fluid dynamic problems, BEMs are utilised in order to handle complicated geometries, such as ship hulls or aircraft, and to calculate the force applied from the fluid to a body (floating or fully submerged body). The part of the body surface in contact with the fluid (the wetted-body surface) is discretized into panels and the problem is formulated in a boundary integral equation form via Green's theorem [1] [6] [7]. A number of commercial software codes have been developed to resolve BVPS via BEMs, in both frequency domain (e.g. NEMOH, WAMIT, Aquaplus, Aqwa and WADAM) and time domain (e.g. ACHIL3D).

The algorithms of the BEMs calculate, as a result, the added mass matrix $\mathbf{A}$, the radiation damping matrix $\mathbf{B}$, and the excitation force transfer function matrix $\mathbf{H_{f_e}}$, associated with the specific body geometry. The hydrodynamic matrices ($\mathbf{A}$, $\mathbf{B}$ and $\mathbf{H_{f_e}}$), calculated for the panelised body surface, converges to the hydrodynamic matrices associated with the original (non panelised) body surface, by reducing the panel size. Therefore, it is clear that the calculated hydrodynamic parameters depend on the utilised mesh, and the results are more accurate for finer meshes. On the other hand, the disadvantage of a high resolution mesh is the larger required computation time for the BEM solution calculation. The balance between the time constraint and the required accuracy has to be the result of a pragmatic compromise.

A way to observe the level of convergence of the mesh is the comparison of hydrodynamic curves, calculated by utilising different panel sizes (and therefore different panel numbers). Indeed, the utilised mesh can be considered sufficiently fine, if a further mesh resolution increment does not bring significant changes in the calculated BEM hydrodynamic curves. In the case of a single floating body with 6 degrees of freedom (DoF), 36 different added mass curves are calculated, together

1279 Wave Hydrodynamic Modelling.

S. Giorgi is with Wave Venture Ltd., Penstraze Business Centre, Cornwall, UK (e-mail: simone.giorgi@wave-venture.com).

R. Costello is with Wave Venture Ltd., Penstraze Business Centre, Cornwall, UK (e-mail: ronan@wave-venture.com).

B. Kennedy is with Wave Venture Ltd., Penstraze Business Centre, Cornwall, UK (e-mail: ben@wave-venture.com).

with 36 different radiation damping curves and 6 excitation force transfer function curves; therefore, even in the case of a single body, the visual inspection of the BEM results could be long and onerous. Furthermore, in the case of multiple body WECs or WEC arrays, the number of the hydrodynamic curves to inspect could increase considerably. For example, in the case of an array with 20 bodies, the visual inspection would involve 14,400 hydrodynamic curves only for the added mass matrix! It is clear that the visual inspection of BEM hydrodynamic parameters could be too arduous and time consuming; therefore, the use of metrics for an automatic convergence analysis is very desirable.

In the literature, different studies show the dependence of the BEM results versus the mesh panel number. In [8], the BEM software packages WAMIT and NEMOH are utilised to calculate the hydrodynamic parameters of four typical wave energy converting concepts. A mesh convergence study shows the dependency of the radiation damping versus the panel number. In [9], a higher-order boundary element method is implemented to study the interaction of an impulse wave propagating in a circular cylindrical tank, with a surface-piercing cylinder located at its centre. The presence of incident, diffracted and reflected waves results in a rather complex free surface dynamics. Three different mesh resolutions are utilised for the calculation of the time history of wave elevation at the front of the cylinder, and the force applied on the cylinder. In [10], a computational example of a diffraction problem is provided, where the surge force and yaw moment are calculated in the case of a spar buoy, which consists of a cylindrical surface and three helical strakes. Three different meshes, characterised by different panel numbers, are utilised to resolve the problem. In [11], the heave added mass hydrodynamic curve is calculated for a McIver toroid, by utilising three different mesh resolutions. In [12], a non-axisymmetric trapping structure, composed by joining together toroids of different radius, is modelled by using the BEM software WAMIT. Three different meshes, characterised by different resolutions, are utilised in order to calculate the heave added mass curve. In [13], the hydrodynamic response analysis (at zero forward speed) of a hybrid marine vehicle, namely HDV-100, is carried out. Three meshing schemes, with different panel sizes, are provided to the BEM code HYDRAN, which is developed specially to analyse the three-dimensional hydroelastic response of marine structures.

The presented methodology is applied in this work, by using the hydrodynamic data generated by the BEM software package NEMOH [14] [15], developed by the Ecole Centrale de Nantes. The case study, presented in this work, is based on floating bodies, but the same methodology can be applied to fully submerged bodies.

The paper is laid out as follows; Section II describes the proposed mesh convergency frame, with Sections II-A and II-B illustrating the vector and matrix norms utilised for this paper. Section II-C introducing the concept of significance hydrodynamic mode-maps, Section II-D defining the metric utilised to measure total variation between hydrodynamic matrices having different mesh resolutions, Section III documents a case study showing the results of such a procedure, for the case of an array composed by 12 floating vertical cylinders. Finally, conclusions are drawn in Section IV.

II. Proposed mesh convergence framework

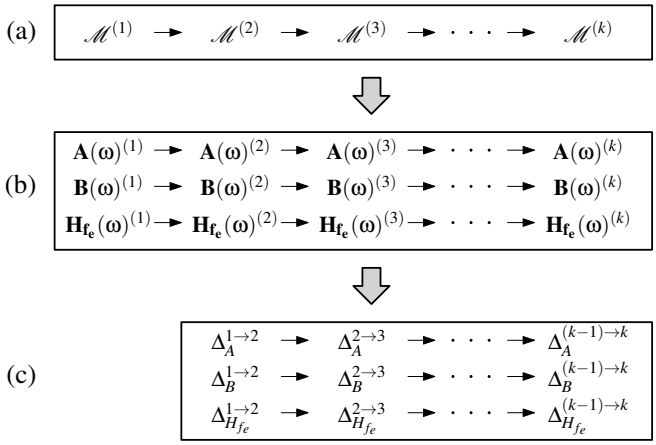

Fig. 1. Conceptual steps for the measure of the mesh convergence: (a) Generation of a sequence of meshes, having an increasing resolution, (b) Calculation, by a BEM software, of the associated hydrodynamic parameters and (c) Calculation of the sequence of numbers (provided by a specified metric), representing the variation of the hydrodynamic characteristics for two different mesh resolutions.

This section presents the construction of the proposed metric, which can be utilised in order to measure the level of convergence of the hydrodynamic curves, for different mesh resolutions. Given the geometry of an array of bodies, the idea is based on the generation of a sequence of meshes $\mathscr{M}^{(1)}$, $\mathscr{M}^{(2)}$, ..., $\mathscr{M}^{(k)}$ (having increased mesh resolution), utilised to discretize the wetted-body surface of the array (see Fig. 1-a). At each k-th step, the metric should be used to decide if a finer mesh, $\mathscr{M}^{(k+1)}$, is necessary, or if the mesh convergence has already been reached. A multiplicity of different criteria could be utilised to define the metric, depending on which specific necessities are taken in consideration. In this paper, the convergence mesh measure is not directly carried out on the mesh itself, but studying how variation of the mesh is related to variations of the hydrodynamic matrices. Indeed, each k-th mesh, $\mathscr{M}^{(k)}$, is associated with the k-th hydrodynamic matrices $\mathbf{A}^{(k)}$, $\mathbf{B}^{(k)}$ and $\mathbf{H_{fe}}^{(k)}$; therefore, the original mesh sequence generates hydrodynamic matrix sequences (see Fig. 1-b). The use of a metric, able to measure the variation between two contiguous elements of a hydrodynamic matrix sequence (such as $\mathbf{A}^{(1)}$ and $\mathbf{A}^{(2)}$), generates a sequence of positive real numbers (see Fig. 1-c). When the k-th element of the sequence is close to zero, the associated matrix is not significantly changing any more and the hydrodynamic curves have sufficiently converged.

A. Norm metrics

Given a (real or complex) signal $s(\xi)$, a sampling period Δ, and an integer k, the signal sample $s(k\Delta)$,

in this paper, is denoted $s(k)$ in order to simplify the notation. The sequence of N_k signal samples, $\mathbf{s} = [s(1), s(2), ..., s(N_k)]$, is just a sequence of (real or complex) numbers, which can be interpreted as the components of a vector. Therefore, different vector norms can be utilised in order to quantify the 'magnitude' of the sampled signal. The most utilised vector norms are the infinity norm and the p-norm, defined respectively by [16] [17]:

$$\| \mathbf{s} \|_{\infty} = \max_{k} \left| s(k) \right| \qquad \text{with} \quad k = 1, ..., N_k \tag{1}$$

and

$$\| \mathbf{s} \|_{p} = \left[\sum_{k=1}^{N_k} s^p(k) \right]^{1/p} \tag{2}$$

In particular, the p-norm of equation (2) becomes the well know Euclidean norm (also called 2-norm) for $p = 2$. It is interesting to note that the infinity norm, given by equation (1), is very sensitive to any sporadic maximum peak, whereas, the p-norm (2) is more representative of the whole signal. One of the objectives of this paper is to 'measure' the characteristics of the whole hydrodynamic curves, consequently, only the 2-norm is implemented in the case study of Section III.

B. Metric to measure the significance of a matrix element

This section, given a real or complex matrix $\mathbf{G} = \left[g(p,q) \right]$ with dimension $N_p \times N_q$, introduces a metric to quantify if the absolute value of an element of $\mathbf{G}$ is large enough to be considered significant with respect to the other $\mathbf{G}$ elements. The main idea is to compare each matrix element with a quantity utilised to describe the average magnitude of the matrix. The calculation of the relevance of each matrix element can be carried out in a sequence of steps:

1) Calculation of the maximum of the absolute value (or of the module, in the case of complex numbers) of all the matrix elements, which for definition is the max-norm of the matrix, given by [17]:

$$\| \mathbf{G} \|_{max} = \max_{p,q} \left| g(p,q) \right| \tag{3}$$

where $p = 1, ..., N_p$ and $q = 1, ..., N_q$.

2) Calculation of the new matrix $\widetilde{\mathbf{G}}$, with elements given by:

$$\widetilde{g}(p,q) = \frac{|g(p,q)|}{\| \mathbf{G} \|_{max}} \tag{4}$$

or in a more compact matrix form:

$$\widetilde{\mathbf{G}} = \frac{|\mathbf{G}|}{\| \mathbf{G} \|_{max}} \tag{5}$$

where $|\mathbf{G}|$, in this paper, represents the matrix of the absolute elements $|g(p,q)|$. $\widetilde{\mathbf{G}}$ is a normalised matrix, composed by elements contained in the interval $[0, 1]$.

3) Given a threshold $T_r \geq 0$, an element of $\widetilde{\mathbf{G}}$ is considered significant if

$$\widetilde{g}(p,q) \geq T_r \tag{6}$$

The set $\{(p,q)\}$, made of the index couples of all the significant elements of $\mathbf{G}$, is denoted $\mathscr{S}_G$, and called by the authors of this paper *significant index set*.

C. Significance hydrodynamic mode-maps

Given a system of N_b (floating or bottom-mounted) bodies, and considering 6 DoF for each body (also called modes [18] [19]), the BEM software package calculates the associated hydrodynamic parameter matrices $\mathbf{A}$, $\mathbf{B} \in \mathbb{R}^{6N_b \times 6N_b \times N_k}$ and $\mathbf{H_{f_e}} \in \mathbb{C}^{6N_b \times 1 \times N_k}$, where $\mathbb{R}$ and $\mathbb{C}$ are the real and complex number set, respectively, and N_k is the number of frequencies utilised. The metrics, introduces in Sections II-A and II-B, can be combined in order to calculate the significant modes of the system.

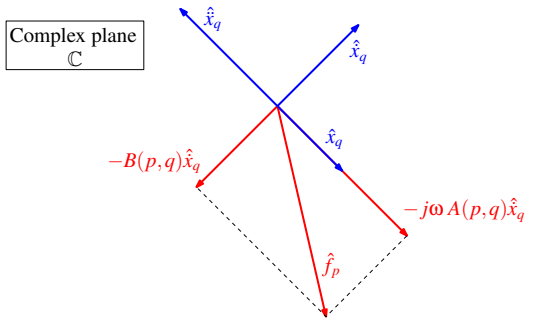

Fig. 2. Radiation force projection diagram, where $\hat{f}_p$ is the complex phasor of radiation force in the p-th mode, j is the imaginary unit and $\hat{x}_q$, $\hat{\dot{x}}_q$ and $\hat{\ddot{x}}_q$ are the complex phasors of the body position, velocity and acceleration, respectively, in the q-th mode.

In general, the hydrodynamic radiation damping term is related to the component of the radiation force in phase with the velocity; whereas, the added mass term is related to the component in quadrature with the body velocity (and in phase with the acceleration), as shown in Fig. 2. Therefore, the index couple (p,q) of the matrices $\mathbf{A}$ and $\mathbf{B}$ specify the mode cross-coupling effect, from the body velocity (in the q-th mode) to the radiation force (in the p-th mode). Once the mode cross-coupling term is selected, by specifying the index couple (p,q), the elements $\mathbf{A}(p,q,k)$, with $k = 1, ..., N_k$, are the samples of the added mass curve at different frequencies (a vector of N_k elements, which is denoted $a_{pq}(k)$ in this paper, as shown in Fig. 3). Equation (1) or (2) can be used to compute the vector norm $||a_{pq}(k)||$. The *reduced matrix* $\mathbf{A}^R \in \mathbb{R}^{6N_b \times 6N_b}$ (where the superscript 'R' stands for 'reduced') is defined by calculating the vector norm $||a_{pq}(k)||$ for each index couple (p,q):

$$\mathbf{A}^R(p,q) = \| \, a_{pq}(k) \, \| \tag{7}$$

By applying equations (5) and (6) to $\mathbf{A}^R$, the *normalised reduced matrix*, $\widetilde{\mathbf{A}^R}$, and the significant index set, $\mathscr{S}_A$, are obtained:

$$\widetilde{\mathbf{A}^R} = \frac{\mathbf{A}^R}{\| \mathbf{A}^R \|_{max}} \quad \xRightarrow{T_r} \quad \mathscr{S}_A \tag{8}$$

Note that the elements of the reduced matrix $\mathbf{A}^R$ are normalised without reference to the units; the objective is the scaling of the element magnitude, not the achievement of a dimensionless matrix. By plotting, on a grid $6N_b \times 6N_b$, a square for each element of $\widetilde{\mathbf{A}^R}$, with a color specified by the element value (which is contained in the interval [0,1]), it is possible to visualize the significance of each mode. The authors of this

paper called this kind of plots *significance hydrodynamic mode-maps*. The same approach can be utilised with $\mathbf{B}$ and $\mathbf{H_{f_e}}$, consequently obtaining the reduced matrices $\mathbf{B}^R \in \mathbb{R}^{6N_b \times 6N_b}$ and $\mathbf{H_{f_e}}^R \in \mathbb{C}^{6N_b \times 1}$ and

$$\widetilde{\mathbf{B}^R} = \frac{\mathbf{B}^R}{\| \mathbf{B}^R \|_{max}} \quad \overset{T_r}{\Longrightarrow} \quad \mathscr{S}_B \tag{9}$$

$$\widetilde{\mathbf{H_{f_e}}^R} = \frac{\mathbf{H_{f_e}}^R}{\| \mathbf{H_{f_e}}^R \|_{max}} \quad \overset{T_r}{\Longrightarrow} \quad \mathscr{S}_{H_{f_e}} \tag{10}$$

Fig. 3 shows an overview of the steps utilised for the construction of the significance hydrodynamic mode-maps. In the case of a large body number N_b, the prediction of the relevant mode cross-coupling terms of the whole system is not banal, but the significance hydrodynamic mode-maps provide a straightforward interpretation.

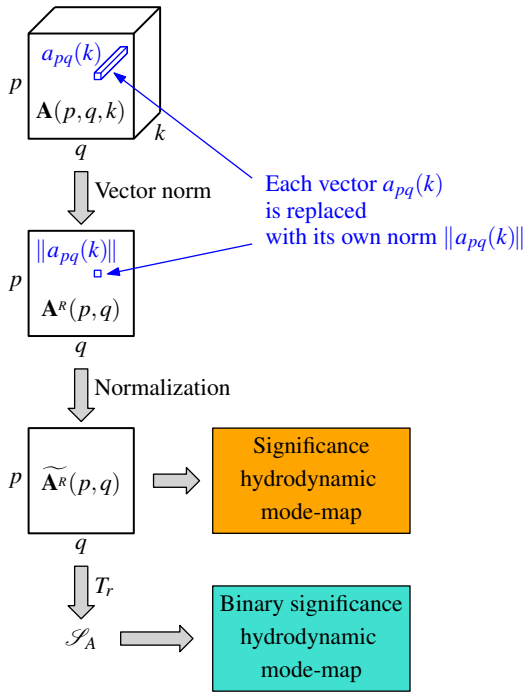

Fig. 3. Steps for the calculation of the significance hydrodynamic mode-maps and binary significance hydrodynamic mode-maps, from the corresponding hydrodynamic matrix (in the case of the added mass matrix $\mathbf{A}$).

D. Metric to measure the matrix variation

Given a sequence of real or complex hydrodynamic matrices $\mathbf{G}^{(1)}$, $\mathbf{G}^{(2)}$, ..., $\mathbf{G}^{(N_m)}$, each one with dimensions $N_p \times N_q \times N_k$, it is desirable to construct a metric in order to measure the variation between $\mathbf{G}^{(n)}$ and $\mathbf{G}^{(n+1)}$, for $n = 1, ..., (N_m - 1)$. The indices p and q specify the hydrodynamic mode cross-coupling term; whereas, the index k specifies the frequency. This work proposes the construction of the metric with the following steps:

1) By choosing the mode cross-coupling term of a matrix, specified by the index couple (p, q), a vector is selected (e.g. $g^{(n)}(p, q, k)$, where the different vector components are given by changing the index k).

2) Define a metric in order to calculate the variation between the vectors $g^{(n)}(p, q, k)$ and $g^{(n+1)}(p, q, k)$ (where k=1,..., N_k), as shown in Fig. 4. In this work, the metric is defined by utilising the 2-norm, given by equation (2):

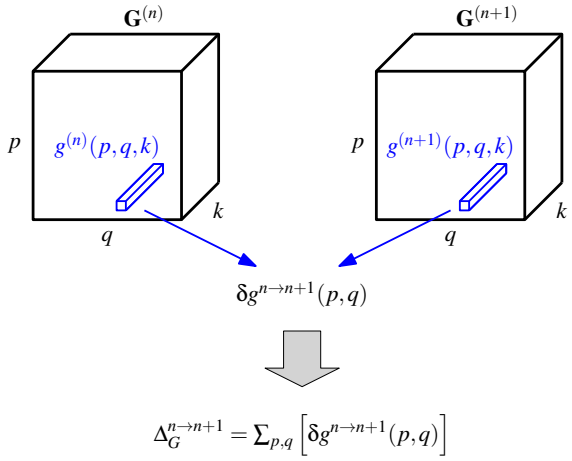

Fig. 4. Block diagram of the hydrodynamic delta matrix metric construction.

$$\delta g^{n\to n+1}(p,q) = \frac{\| g^{(n+1)}(p,q,k) - g^{(n)}(p,q,k) \|_2}{\| g^{(n)}(p,q,k) \|_2} \tag{11}$$

3) The total variation between $\mathbf{G}^{(n)}$ and $\mathbf{G}^{(n+1)}$ can be defined as the summation of the different contributions of $\delta g^{n\to n+1}(p,q)$ for all (p,q):

$$\Delta_G^{n\to n+1} = \sum_{p=1}^{N_p} \sum_{q=1}^{N_q} \left[\delta g^{n\to n+1}(p,q)\right] \tag{12}$$

It is important to note that the definition of equation (11) is based on a ratio; therefore, $\delta g^{n\to n+1}(p,q)$ could be a large value also if the vectors $g^{(n)}(p,q,k)$ and $g^{(n+1)}(p,q,k)$ are not significant in the matrices $\mathbf{G}^{(n)}$ and $\mathbf{G}^{(n+1)}$, respectively. This represents a drawback of the metric, defined with equation (12), since the value calculated by the metric could account contributions from cross-coupling terms, which are negligible from an hydrodynamic point of view. The risk is an overestimate variation calculation, which leads to the request of a further finer mesh, which would not be necessary. In order to eliminate this distortive effect in the metric calculation, only the cross-coupling terms, contained in the significant index set $\mathscr{S}_G$ (see Section II-C), should be taken in consideration for the metric calculation and, consequently, equation (12) should be corrected into:

$$\Delta_G^{n\to n+1} = \sum_{(p,q)\in\mathscr{S}_G} \left(\delta g^{n\to n+1}(p,q)\right) \tag{13}$$

where $\Delta_G^{n\to n+1}$ is termed by the authors of this paper *hydrodynamic delta matrix metric*. By plotting, on a grid $6N_b \times 6N_b$, a coloured square for each element of $\mathscr{S}_G$, it is possible to visualize the significant mode cross-coupling terms (given a specific value of T_r). The authors of this paper called this kind of plots *binary significance hydrodynamic mode-maps*.

III. Case Study

The case study considers an array composed of $N_b = 12$ identical vertical cylinders, having a diameter

$D = 2$ m and a draft $h_d = 5$ m. Each n-th body has a body frames BF_n, having the x-y plane coincident with the undisturbed water surface and the z-axis vertical and positive upwards (see Fig. 5). The 12 bodies are positioned on the regular grid, made of 4 columns and 3 rows, with a distance $L = 8.5$ m between the centres of two adjacent bodies, in both x and y directions; the global frame GF of the whole array is chosen to be coincident with BF_1 (see Fig. 6). In the developed Python code utilised for this work, the body mesh surface of the n-th body is initially defined and constructed with respect BF_n and, successively, it is translated to occupy a body position on the array grid of Fig. 6.

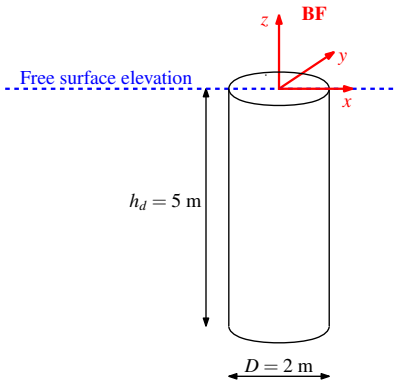

Fig. 5. Single cylinder geometry and body frame (BF) location.

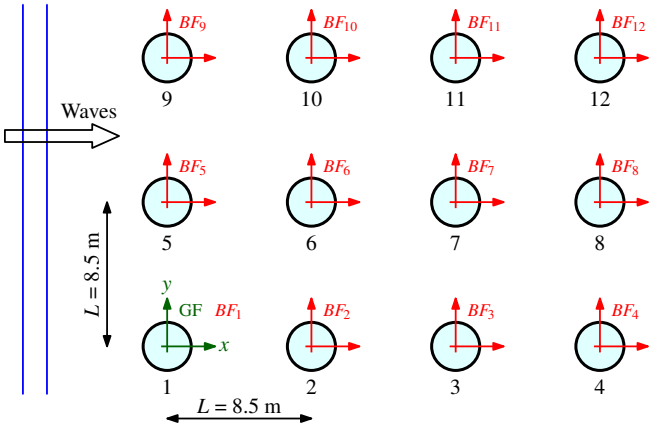

Fig. 6. Top view of the WEC array configuration.

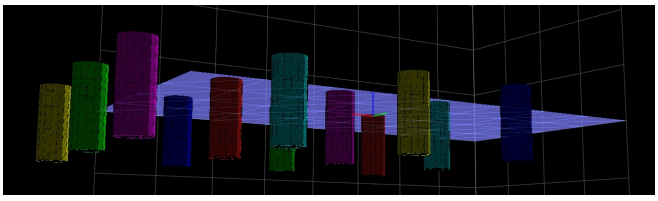

Fig. 7. Implemented 3D array geometry.

The BEM data of the case study are generated by the software package NEMOH, by setting the water density $\rho = 1025$ kg/m^3, the water depth $h_w = 50$ m and 6 DoF for each body (surge, sway, heave, roll, pitch and yaw). For the case study, 5 different meshes are utilised, composed with a number of panels equal to 552, 1640, 3216, 3840 and 4968. Fig. 7 shows the 3D array geometry in the case of 4968 panels. For each NEMOH simulation, the same vector frequency is utilised, which is composed of 64 frequencies, with $\Delta\omega = 1.5\pi/64$ rad/s, $\omega_{min} = 0$ rad/s and $\omega_{max} = (63/64)1.5\pi$ rad/s. Therefore, NEMOH calculates the matrices $\mathbf{A}$, $\mathbf{B} \in \mathbb{R}^{72\times72\times64}$ and $\mathbf{H_{f_e}} \in \mathbb{C}^{72\times1\times64}$, for each mesh resolution. Figs. 8, 9 and 10 show the added mass of the cross-coupling terms (30,30), (34,34) and (34,30), respectively, obtained by NEMOH for the different meshes. It is possible to see that the hydrodynamic curves are extremely similar for the meshes composed with 3216, 3840 and 4968, as shown in particular by the zooms of Fig. 8, which suggest that 3216 panels are sufficient for the added mass in the mode cross-coupling term (30,30).

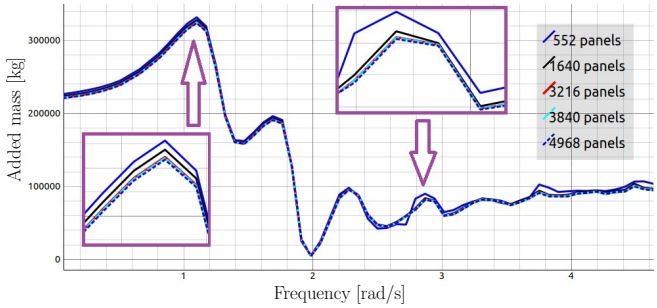

Fig. 8. Added mass hydrodynamic curves for the mode cross-coupling term $(30, 30)$, which corresponds to (surge, surge) of body 6, in the case of the five different utilised meshes. The zooms show that the curves are extremely similar for the meshes composed with 3216, 3840 and 4968.

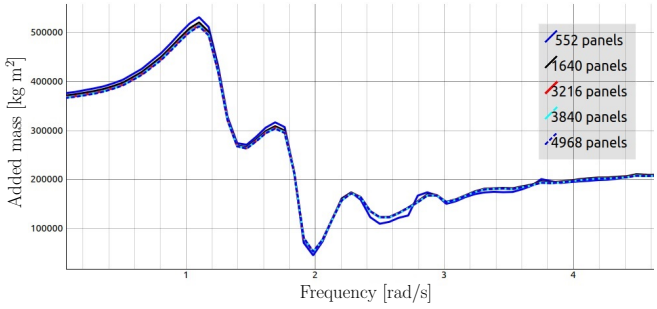

Fig. 9. Added mass hydrodynamic curves for the mode cross-coupling term $(34, 34)$, which corresponds to (pitch, pitch) of body 6, in the case of the five different utilised meshes. The curves are extremely similar for the meshes composed with 3216, 3840 and 4968.

The same kind of visual inspection, performed on the hydrodynamic curves of Figs. 8, 9 and 10, should be carried out for all the 72x72=5184 mode cross-coupling terms of the studied array, in order to verify the convergence of the hydrodynamic curves for different mesh resolutions, clearly an excessive time consuming task. Instead, by following the method proposed in Section II, the hydrodynamic delta metric is utilised to automatically verify the mesh convergence. The matrices $\widetilde{\mathbf{A}^R}$, $\widetilde{\mathbf{B}^R}$ and $\widetilde{\mathbf{H_{f_e}}^R}$ are calculated by utilising equations (8), (9) and (10), respectively. Figs. 11 and 12 show the significance hydrodynamic mode-maps associated with $\widetilde{\mathbf{A}^R}$ and $\widetilde{\mathbf{B}^R}$, respectively, where the intensity of the color is proportional to the importance

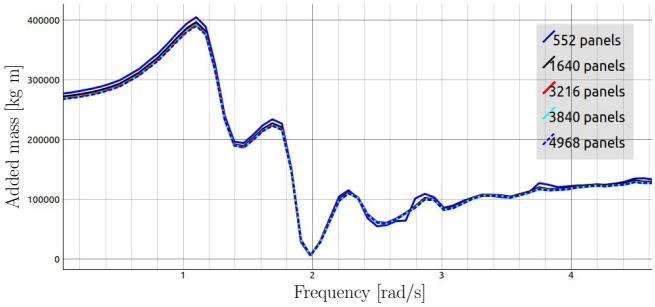

Fig. 10. Added mass hydrodynamic curves for the mode cross-coupling term $(33, 31)$, which corresponds to (roll, sway) of body 6, in the case of the five different utilised meshes. The curves are extremely similar for the meshes composed with 3216, 3840 and 4968.

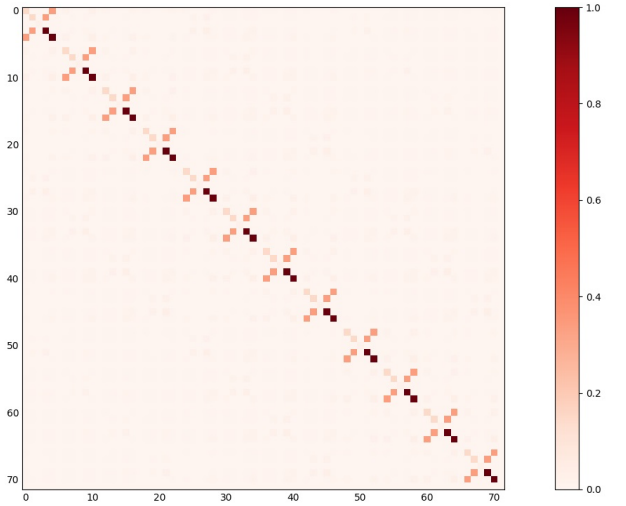

Fig. 11. Significance hydrodynamic mode-map for the added mass matrix $\mathbf{A}$.

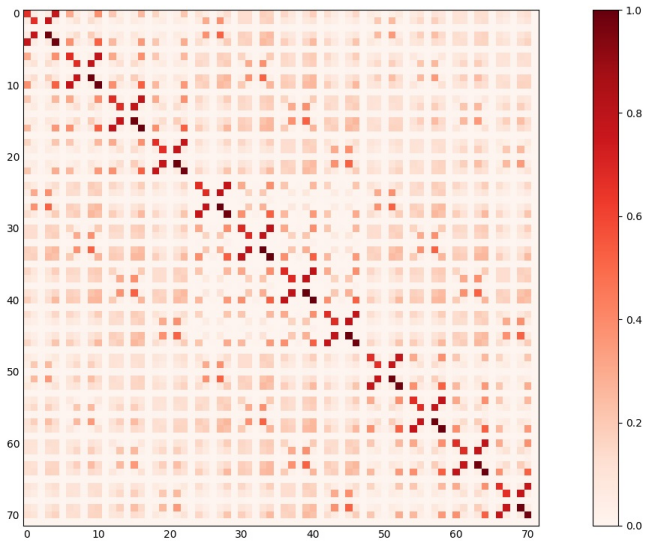

Fig. 12. Significance hydrodynamic mode-map for the radiation damping matrix $\mathbf{B}$.

of the mode for the array hydrodynamics. As explained in Section II-D, the calculation of the hydrodynamic delta matrix metric (13) requires the calculation of the binary significance hydrodynamic mode-map, in order to account only the significant mode cross-coupling terms. Figs. 13 and 15 show the binary significance hydrodynamic mode-maps of $A(\omega)$ and $B(\omega)$, respectively, for three different thresholds $T_r = 0.01,\ 0.1$ and 0.5. Figs. 13(a) and 15(a) show that any cross-coupling term involving the mode yaw (given by the mode indices $5+6m$, for $m = 0, ..., 11$) is totally absent even for the low threshold $T_r = 0.01$, as expected for a vertical cylinder. By increasing the threshold, it is possible to focus on the most relevant mode cross-coupling terms. Figs. 13(b) and 14 show that, in the case of the added mass, the surge to surge and sway to sway are the most important coupling effects between modes of adjacent bodies. Figs. 15(c) and 16 show that, in the case of the radiation damping, the pitch to pitch and roll to roll are the most significant coupling effects between modes of adjacent bodies. The larger coupling effects, between the modes of the same body, are given by surge-pitch and sway-roll coupling, for both added mass and radiation damping, as shown in Figs. 13(c) and 15(c).

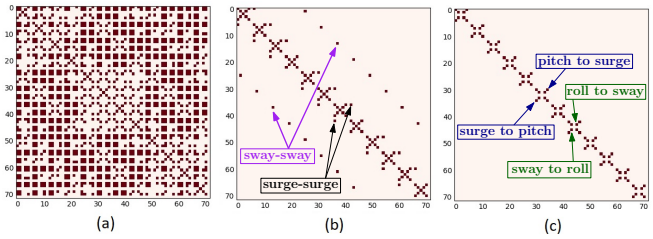

Fig. 13. Binary significance hydrodynamic mode-map (the significant elements are in dark red) for the added mass matrix $\mathbf{A}$, in the case of threshold (a) $T_r = 0.01$. (b) $T_r = 0.1$. (c) $T_r = 0.5$.

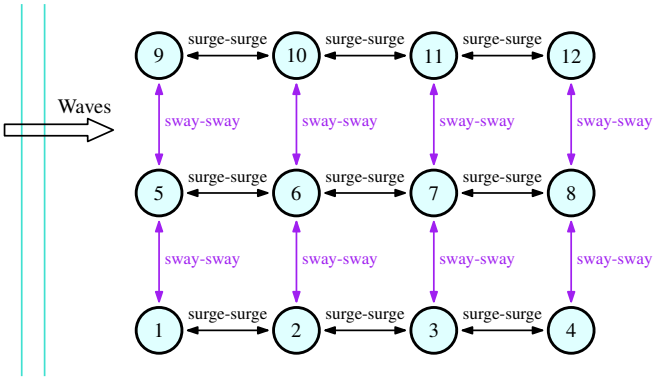

Fig. 14. In the case of the added mass, the most relevant cross-coupling terms, between different bodies of the studied array, are the translational surge-surge and sway-sway coupling.

The hydrodynamic delta matrix metric, defined in (13), is utilised to carry out the convergence mesh study on the added mass and radiation damping matrices, in the case of $Tr = 0.01,\ 0.1$ and 0.5. The convergence speed of the hydrodynamic curves could change for different mode cross-coupling terms. Therefore, by selecting a different T_r (which changes the significant index set, as explained in Section II-C), it is possible

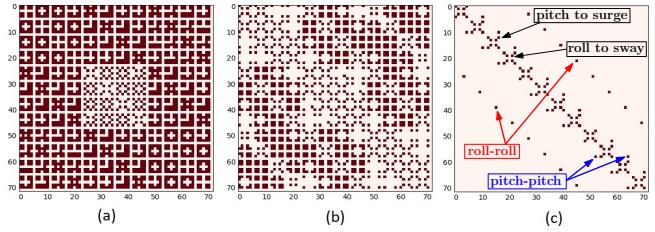

Fig. 15. Binary significance hydrodynamic mode-map (the significant elements are in dark red) for the radiation matrix $\mathbf{B}$, in the case of threshold (a) $T_r = 0.01$. (b) $T_r = 0.1$. (c) $T_r = 0.5$.

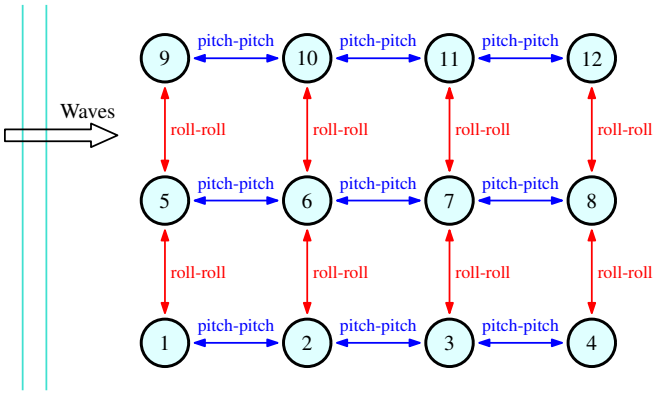

Fig. 16. In the case of the radiation damping, the most relevant cross-coupling terms, between different bodies of the studied array, are the rotational pitch-pitch and roll-roll coupling.

to account, in the convergence analysis, modes having different importance in the array hydrodynamics. The use of a threshold close to zero (such as 0.01 in the present case study) provides a general overview regarding the convergence speed of the hydrodynamic matrices, since most of the modes are accounted in equation (13), as shown in Figs. 13(a) and 15(a). Fig. 17 shows that, in the case of $T_r = 0.01$, by passing from 1640 to 3216 panels, the variation of the hydrodynamic curves is clearly less relevant than by passing from 552

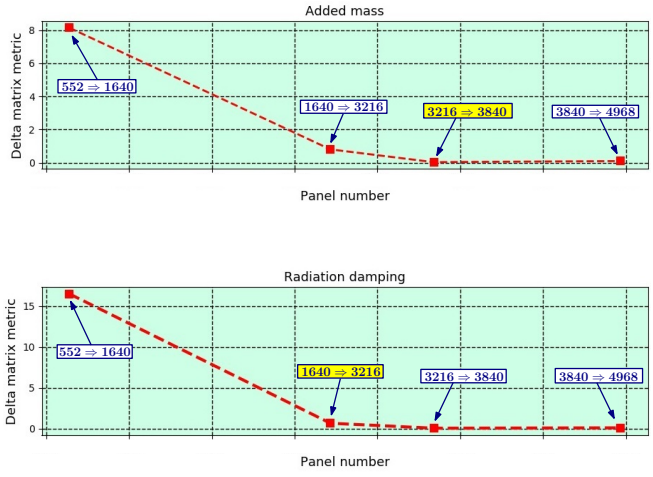

Fig. 17. Delta matrix metric calculation for the added mass and radiation damping matrices, in the case of $T_r = 0.01$. The first panel number increment, which results in no significant improvement of the hydrodynamic curve, is marked in yellow. The increase from 3216 to 3840 panels (for the added mass) and from 1640 to 3216 panels (for the radiation damping) bring no significant improvement.

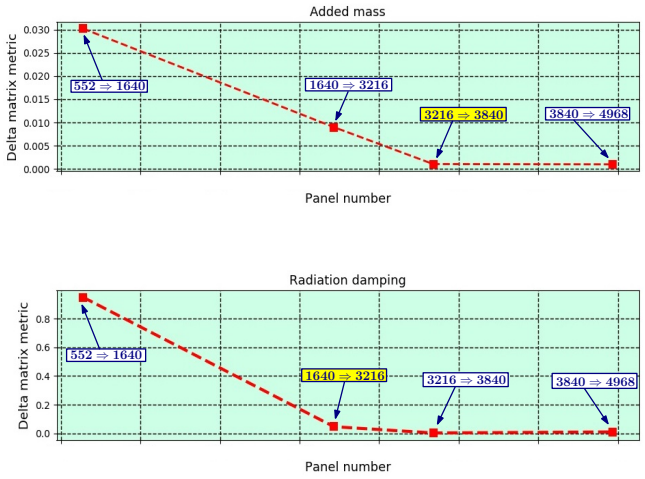

Fig. 18. Delta matrix metric calculation for the added mass and radiation damping matrices, in the case of $T_r = 0.1$. The first panel number increment, which results in no significant improvement of the hydrodynamic curve, is marked in yellow. The increase from 3216 to 3840 panels (for the added mass) and from 1640 to 3216 panels (for the radiation damping) bring no significant improvement.

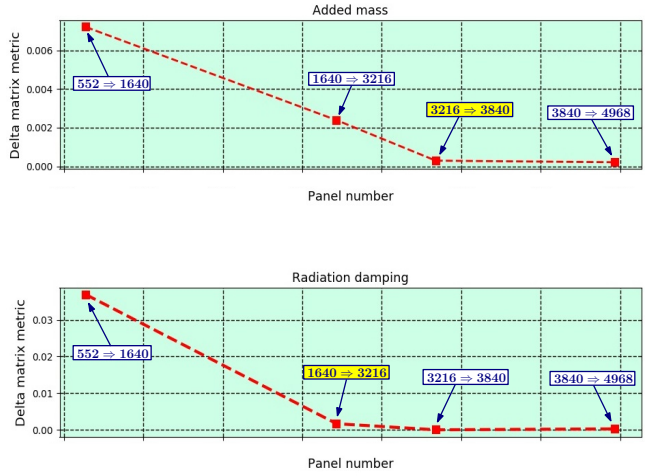

Fig. 19. Delta matrix metric calculation for the added mass and radiation damping matrices, in the case of $T_r = 0.5$. The first panel number increment, which results in no significant improvement of the hydrodynamic curve, is marked in yellow. The increase from 3216 to 3840 panels (for the added mass) and from 1640 to 3216 panels (for the radiation damping) bring no significant improvement.

to 1640 panels. However, in the case of the added mass, the panel number transition $1640 \Rightarrow 3216$ represents a significant, even if small, improvement. Therefore, the first panel number increment, which results in no significant improvement of the hydrodynamic curves, is $3216 \Rightarrow 3840$ panels (for the added mass) and $1640 \Rightarrow 3216$ panels (for the radiation damping). By increasing T_r, the less important hydrodynamic modes are excluded in the calculation of the metric (13). Figs. 18 and 19, related to $Tr = 0.1$ and 0.5, respectively, both show that the first panel number increment, which results in no significant improvement of the hydrodynamic curve, is $3216 \Rightarrow 3840$ panels (for the added mass) and $1640 \Rightarrow 3216$ panels (for the radiation damping). Therefore, for the proposed case study, a mesh with 3216 panels represents a good compromise for the BEM mesh resolution. Note that the same conclusion was reached by visual inspection

of the mode cross-coupling terms (30,30), (34,34) and (33,31) in Figs. 8, 9 and 10, respectively.

IV. Conclusions

A new metric is defined to implement an automatic convergence analysis of BEM results, in order to avoid the necessity of carrying out time consuming visual inspection of the hydrodynamic curves. The paper also introduces the concept of "significance hydrodynamic mode-maps", in order to visualize the most relevant mode cross-coupling terms of a multiple body system. The proposed tools are applied for the convergence mesh study of an array, composed of 12 identical floating vertical cylinders, by utilising five different meshes, composed of 552, 1640, 3216, 3840 and 4968 panels, respectively. The results show that, for the chosen array, the use of a mesh with a number of panels equal to 3216 represents a good compromise for the BEM mesh resolution; indeed, the mesh with 3216 panels can be considered converged, since a farther increment of the panel number introduces no significant improvement in the hydrodynamic curves.

An interesting future work is the use of different normalizing terms (due to the presence of elements with difference units in the hydrodynamic matrices) for the calculation of the normalised reduced matrices. Indeed, in some particular cases (such as very long vertical cylinders), large numerical differences between the elements with different units could lead to a possible evanescence of some relevant modes from the calculated hydrodynamic mode-maps.

References

[1] Y. Liu, *Fast Multipole Boundary Element Method: Theory and Applications in Engineering*. Cambridge University Press, 2009.

[2] R. Dean and R. Dalrymple, *Water Wave Mechanics for Engineers and Scientists*, ser. Advanced Series on Ocean Engineering. World Scientific Publishing Company, 1991.

[3] A. H.-D. Cheng and D. T. Cheng, "Heritage and early history of the boundary element method," *Engineering Analysis with Boundary Elements*, vol. 29, no. 3, pp. 268–302, 2005.

[4] P. Schmitt, K. Doherty, D. Clabby, and T. Whittaker, "The opportunities and limitations of using CFD in the development of wave energy converters," in *Proceedings of the Marine and Offshore Energy Conference*, 2012.

[5] S. Kirkup, J. Yazdani, N. Mastorakis, M. Poulos, V. Mladenov, Z. Bojkovic, D. Simian, S. Kartalopoulos, A. Varonides, and C. Udriste, "A gentle introduction to the boundary element method in matlab/freemat," in *Proceedings of the WSEAS International Conference. Proceedings. Mathematics and Computers in Science and Engineering*, no. 10. WSEAS, 2008.

[6] G. Beer, I. Smith, and C. Duenser, *The Boundary Element Method with Programming: For Engineers and Scientists*. Springer Vienna, 2008.

[7] Q. Ma, *Advances in Numerical Simulation of Nonlinear Water Waves*, ser. Advances in coastal and ocean engineering. World Scientific, 2010.

[8] M. Penalba, T. Kelly, and J. V. Ringwood, "Using nemoh for modelling wave energy converters: A comparative study with wamit," *Centre for Ocean Energy Research (COER), Maynooth University, Co. Kildare, Ireland*, 2017.

[9] W. Bai and R. E. Taylor, "Higher-order boundary element simulation of fully nonlinear wave radiation by oscillating vertical cylinders," *Applied Ocean Research*, vol. 28, no. 4, pp. 247–265, 2006.

[10] C. Lee and J. Newman, "Computation of wave effects using the panel method," *Numerical Models in Fluid Structure Interaction*, vol. 42, pp. 211–251, 2005.

[11] Lee and Newman, "Solution of radiation problems with exact geometry," in *Proc. 16th Intl. Workshop on Water Waves and Floating Bodies. Hiroshima, Japan*, 2001, pp. 93–96.

[12] P. McIver and J. Newman, "Non-axisymmetric trapping structures in the threedimensional water-wave problem," in *Proceedings 16th International Workshop on Water Waves and Floating Bodies*, 2001.

[13] H. Zhou, "Hydrodynamic response of an advanced marine vehicle in waves," *Ocean and Resources Engineering*, pp. 9–22, 2003.

[14] A. Babarit and G. Delhommeau, "Theoretical and numerical aspects of the open source BEM solver NEMOH," in *Proceedings of the 11th European Wave and Tidal Energy Conference*, 2015.

[15] LHEEA Centrale Nantes, "Nemoh-presentation," https://lheea.ec-nantes.fr/software-and-patents/nemoh-presentation-217691.kjsp?RH=1489593406974, Feb. 2019.

[16] G. Golub and C. Van Loan, *Matrix Computations (4th Edition)*, ser. Matrix Computations. Johns Hopkins University Press, Baltimore, Maryland, USA, 2012.

[17] X. Yang, *Introduction to Mathematical Optimization: From Linear Programming to Metaheuristics*. Cambridge International Science Publishing, 2008.

[18] J. Falnes, *Ocean Waves and Oscillating Systems, Linear Interactions Including Wave-Energy Extraction*. Cambridge University Press, 2002.

[19] C. H. Lee, "Wamit theory manual," Tech. Rep., 1995.